Supporting Information

to accompany

8-HaloBODIPYs and Their 8-(C, N, O, S) Substituted Analogues: Solvent Dependent UV–vis Spectroscopy, Variable Temperature NMR, Crystal Structure Determination, and Quantum Chemical Calculations

Noël Boens,[a, *] **Lina Wang**,[a,b] **Volker Leen**,[a] **Peijia Yuan**,[a,c] **Bram Verbelen**,[a] **Wim Dehaen**,[a] **Mark Van der Auweraer**,[a] **Wim D. De Borggraeve**,[a] **Luc Van Meervelt**,[a] **Jeroen Jacobs**,[a] **David Beljonne**,[d] **Claire Tonnelé**,[d] **Roberto Lazzaroni**,[d] **Maria J. Ruedas-Rama**,[e] **Angel Orte**,[e] **Luis Crovetto**,[e] **Eva M. Talavera**,[e] **Jose M. Alvarez-Pez**[e]

[a] *Department of Chemistry, Katholieke Universiteit Leuven, Celestijnenlaan 200f – bus 02404, 3001 Leuven, Belgium*

[b] *Current affiliation: College of Environment and Safety Engineering, Qingdao University of Science and Technology, Qingdao, Shandong province 266042, China*

[c] *Current affiliation: Department of Chemistry, Yale University, New Haven, CT 06520, USA*

[d] *Laboratory for Chemistry of Novel Materials, Université de Mons, Place du Parc 20, 7000 Mons, Belgium*

[e] *Department of Physical Chemistry, University of Granada, Cartuja Campus, 18071 Granada, Spain*

Contents

[*] Corresponding author: E-mail: Noel.Boens@chem.kuleuven.be

Experimental section

Instrumentation

The absorption measurements were performed on a Perkin-Elmer Lambda 40 UV-vis spectrophotometer. Fully corrected, steady-state fluorescence excitation and emission spectra were recorded on a SPEX Fluorolog instrument. ^{1}H-NMR spectra were recorded on a Bruker Avance 600 instrument operating at a frequency of 600 MHz. ^{13}C-NMR spectra were recorded at room temperature on a Bruker Avance 300 instrument operating at a frequency of 75 MHz. ^{1}H-NMR spectra in $CDCl_3$ were referenced to tetramethylsilane (0.00 ppm) as an internal standard. ^{13}C-NMR spectra in $(CD_3)_2SO$ were referenced to the $(CD_3)_2SO$ (39.52 ppm) signal. Chemical shifts multiplicities are reported as s = singlet, d = doublet, m = multiplet. Due to the small coupling constants in pyrroles and pyrrolic dyes, the multiplicity of the signals is often unclear. In these cases, signals often appear as singlets, while they are not. Mass spectra were recorded on a Hewlett-Packard 5989A mass spectrometer (EI mode). High-resolution mass data were obtained with a Kratos MS50TC instrument. Melting points were taken on a Reichert Thermovar and are uncorrected.

Crystal structure determination

Yellow single crystals of **7**, **8**, and **10**, suitable for X-ray diffraction were obtained by slow diffusion of pentane into a dichloromethane solution of the compounds at room temperature over a two week period. X-ray intensity data were collected at 100K on an Agilent Supernova diffractometer, equipped with an Atlas CCD detector, using Mo Kα radiation (λ = 0.71073 Å). The images were interpreted and integrated with the CrysAlis PRO software from Agilent.[1] Using Olex2,[2] the structure was solved with the ShelxS[3] structure solution program using Direct Methods and refined with the ShelxL[3] refinement package using full-matrix least squares minimization on F^2. Non-hydrogen atoms were refined anisotropically. Hydrogen atoms were found in difference electron density maps and refined isotropically. The crystallographic data of **7**, **8**, and **10** are compiled in Table S3. CCDC 961709 (**7**), CCDC 961710 (**8**), and CCDC 961708 (**10**) contain the supplementary crystallographic data for this paper and can be obtained free of charge via www.ccdc.cam.ac.uk/conts/retrieving.html (or from the Cambridge Crystallographic Data Centre, 12, Union Road, Cambridge CB2 1EZ, UK; fax: +44-1223-336033; or deposit@ccdc.cam.ac.uk).

Relative determination of fluorescence quantum yield Φ

For the relative determination of the fluorescence quantum yield Φ in a series of solvents, the following formula (eq S1) was used:

$$\Phi_x = \Phi_r \times \frac{F_x}{F_r} \times \frac{1-10^{-A_r(\lambda_{ex})}}{1-10^{-A_x(\lambda_{ex})}} \times \frac{n_x^2}{n_r^2} \qquad \text{(S1)}$$

The subscripts x and r refer respectively to sample x (i.e., BODIPY derivatives) and reference (standard) fluorophore r with known quantum yield Φ_r in a specific solvent, F stands for the *spectrally corrected*, integrated fluorescence spectra, $A(\lambda_{ex})$ denotes the absorbance at the used excitation wavelength λ_{ex}, and n represents the refractive index of the solvent (in principle at the average emission wavelength). To minimize inner filter effects, the absorbance at the excitation wavelength λ_{ex} was kept under 0.1. The measurements were performed using 10 mm optical path length cuvettes under right-angle (L-) arrangement and 'magic angle' conditions. Fluorescein in 0.1 N NaOH (Φ_r = 0.90), coumarin 1 in ethanol (Φ_r = 0.64, acridine yellow G in methanol (Φ_r = 0.57), rhodamine 6G in methanol (Φ_r = 0.86), and quinine sulfate in 0.1 M H_2SO_4 (Φ_r = 0.54) were used as fluorescence quantum yield references. All measurements were done on non-degassed samples at 20 °C. The averages and standard uncertainties of Φ reported in Tables 1 and 2 are usually computed from 12 independent Φ measurements, resulting from 3 conc. of sample x × 2 conc. of reference r × 2 excitation wavelengths λ_{ex}.

Time-resolved fluorescence

Fluorescence decay traces were recorded by the single photon timing (also called time-correlated single photon counting, TCSPC) method, using the FluoTime200 fluorometer (PicoQuant GmbH). The excitation source, depending on the compound probed, consisted of either a 404 nm (model EPL405, Edinburgh Instruments) picosecond pulsed diode laser, operated at 10 MHz, with a full width at half maximum of 90 ps, or 440 nm, or 532 nm pulsed diode laser (LDH series from PicoQuant GmbH) with a minimum pulse width of 70 ps, and 78 ps, respectively, and operated at a pulse repetition rate of 20 MHz. Fluorescence decay histograms were collected at three different emission wavelengths selected by a grating monochromator, after a polarizer set at the 'magic angle' to avoid polarization artifacts. The fluorescence decay traces were collected over 1320 channels, with a time increment of 36 ps per channel, until they reached 2×10^4 counts in the peak channel. Histograms of the instrument response functions were collected using a LUDOX scatterer.

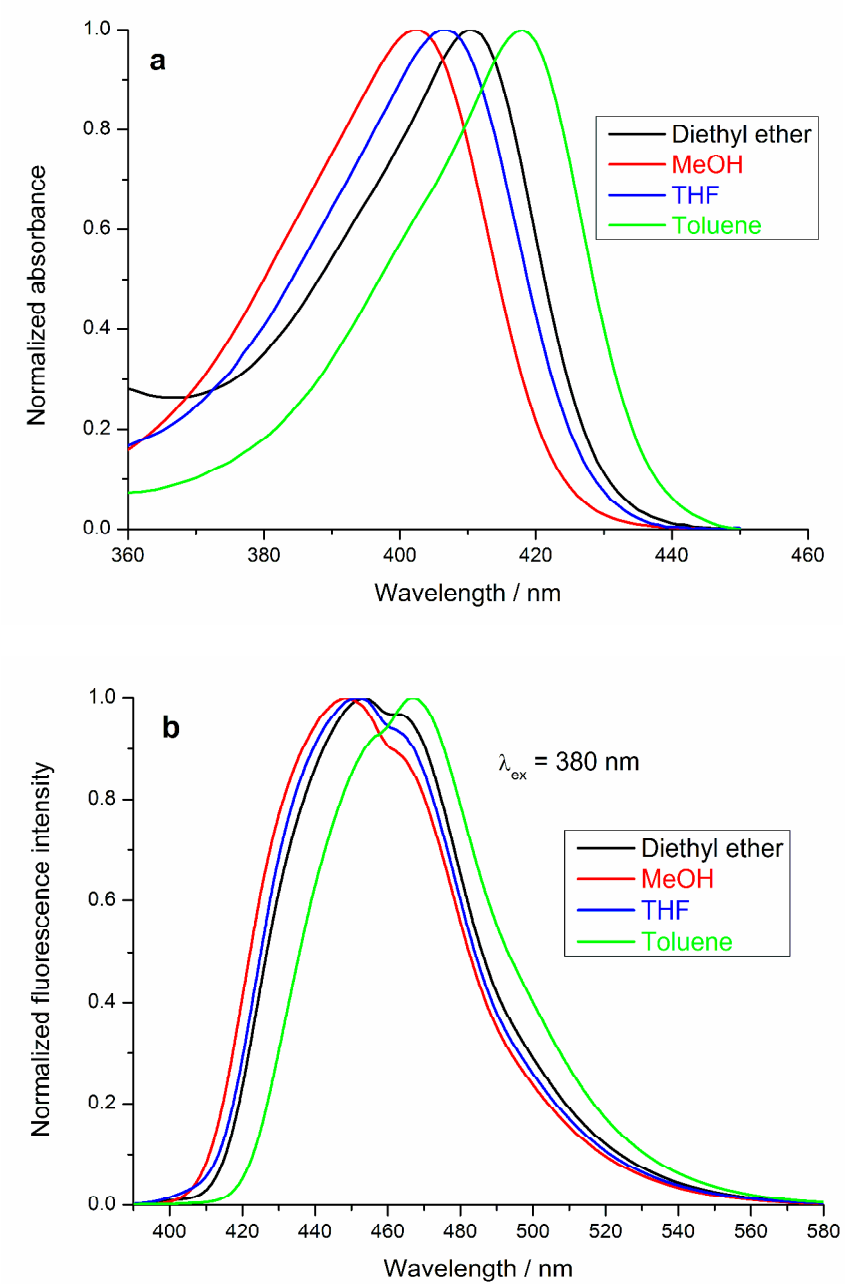

Figure S1. (a) Normalized, visible absorption spectra of **8** in the solvents indicated. (b) Corresponding normalized fluorescence emission spectra upon excitation at 380 nm.

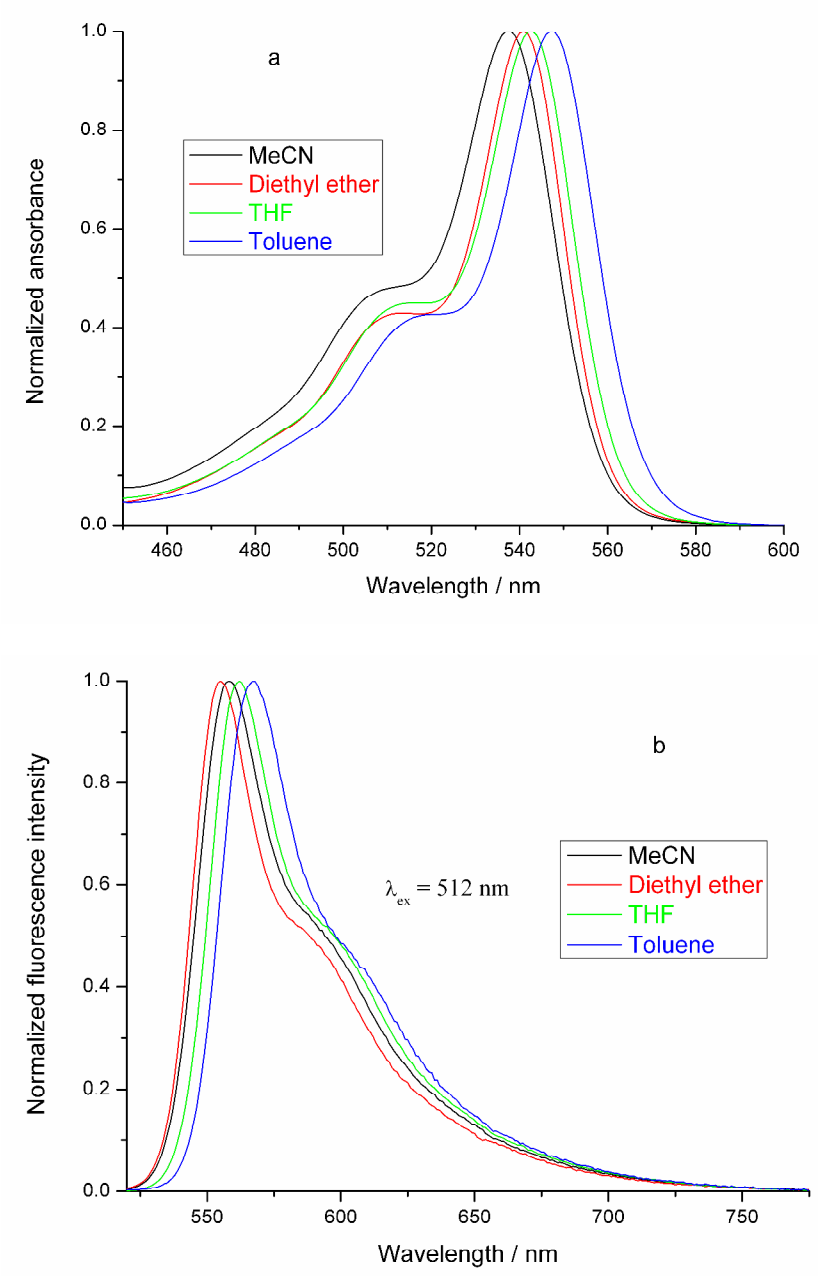

Figure S2. (a) Normalized, visible absorption spectra of **6** in the solvents indicated. (b) Corresponding normalized fluorescence emission spectra upon excitation at 512 nm.

Fluorescence decay histograms

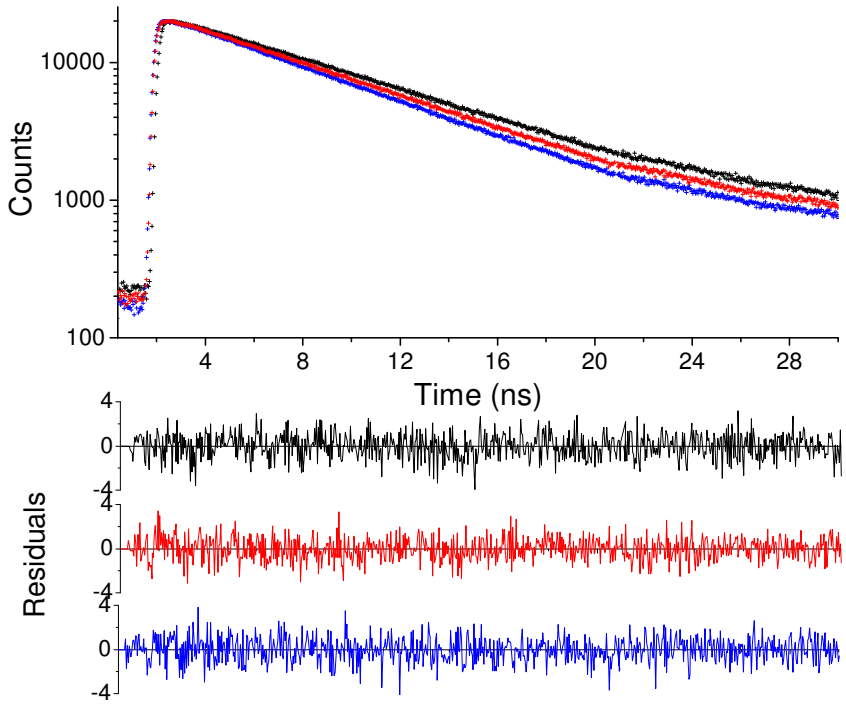

Figure S3. Fluorescence decay traces and corresponding weighted residuals from mono-exponential fits of **6** in diethyl ether (black), dibutyl ether (red), and chlorobenzene (blue). λ_{ex} = 532 nm, λ_{em} = 555 nm.

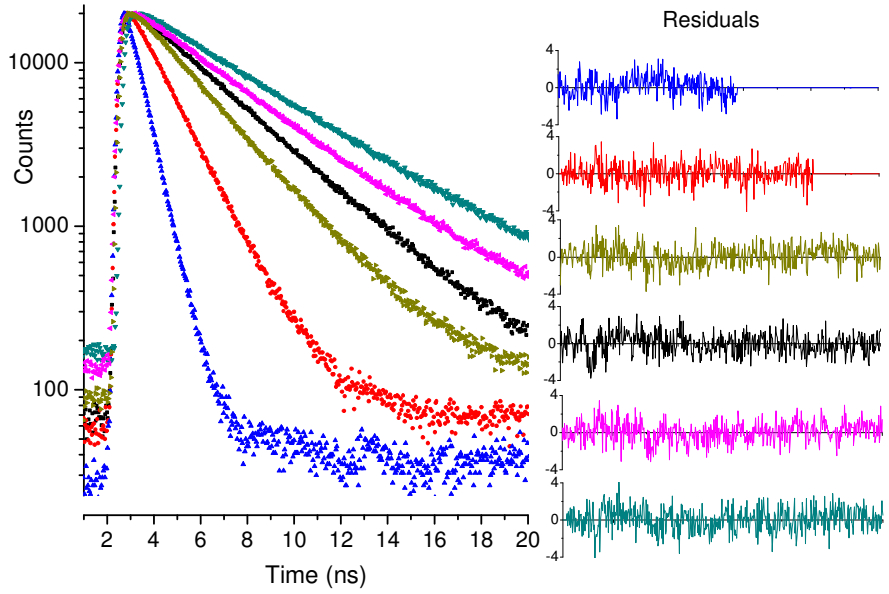

Figure S4. Fluorescence decay traces and corresponding weighted residuals from mono-exponential fits of **8** in methanol (blue), acetone (red), THF (dark yellow), butanenitrile (black), chlorobenzene (pink), and diethyl ether (teal). λ_{ex} = 404 nm, λ_{em} = 460 nm.

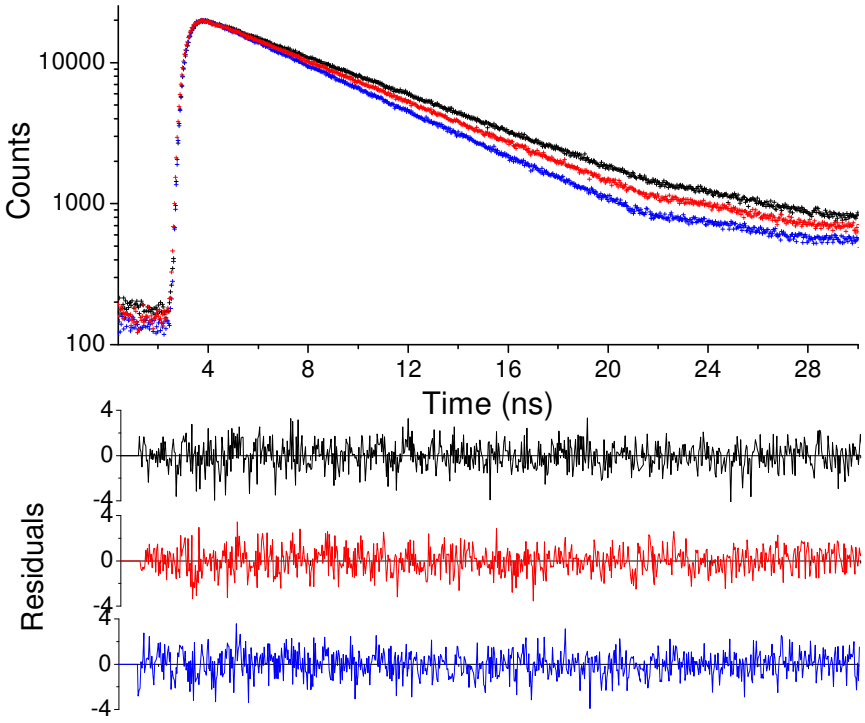

Figure S5. Fluorescence decay traces and corresponding weighted residuals from mono-exponential fits of **10** in diethyl ether (black), dibutyl ether (red), and chlorobenzene (blue). λ_{ex} = 440 nm, λ_{em} = 490 nm.

Solvatochromism

The interactions of the solvent with a solute have been empirically parameterized by a large number of solvent scales. The most frequently used (and well-known) single parameters to describe the nonspecific (also called general) contribution to the solvent effect experienced by any solute are possibly $E_T(30)$,[4, 5, 6] Kamlet, Abboud and Taft's π^* parameter,[7] Dragos' *S*' scale,[8] and Catalán and coworkers' SPP scale.[9] Solvent-dependent spectral shifts are often analyzed in terms of such a single parameter. However, empirical single-parameter solvent scales regularly appear to be inappropriate because that specific parameter is so dependent on the particular probe used to construct the single-parameter scale concerned that it fails to predict the behavior of other solutes with considerably different properties from those of the probe.[10] Multi-parameter approaches, which use multiple scales to describe specific and general solvent effects, have been applied successfully to various physicochemical properties.[11] However, a solvatochromic behavior which is exclusively caused by changes in solvent polarizability cannot be accurately described by e.g. the Kamlet, Abboud and Taft's π^* parameter because this parameter reflects the combined effect of solvent dipolarity and polarizability. To solve this problem, it is necessary to split the two contributions of the general solvent effect, namely solvent dipolarity and polarizability and, hence, to establish two corresponding, independent solvent scales for nonspecific solvent-solute interactions. This was done by Catalán,[10] who proposed the generalized treatment of the solvent effect based on a set of four empirical, complementary, mutually independent solvent scales [for solvent polarizability (SP), dipolarity (SdP), acidity (SA), and basicity (SB)].

Compound 6

Use of the Catalán solvent parameter set {SA, SB, SP, SdP} (eq 1) gives excellent fits to $\bar{\nu}_{abs}$ of **6** using *r* as goodness-of-fit criterion (*r* = 0.979, Table S1). Similarly, good-quality fits are also found for the multi-linear analysis of $\bar{\nu}_{em}$ according to eq 1 (*r* = 0.933, Table S1).

Next, we use the Catalán methodology to unravel which solvent property is primarily responsible for the observed shifts of $\bar{\nu}_{abs}$. The relatively large estimates of c_{SP} and d_{SdP} and their high precision (i.e., comparatively small standard errors) in relation to {a_{SA}, b_{SB}} point to solvent polarizability and dipolarity as major parameters influencing the position of $\bar{\nu}_{abs}$. If either SP or SdP were left out as independent variable in the analyses of $\bar{\nu}_{abs}$ according to eq 1 (that is, with {SA, SB, SdP} and {SA, SB, SP}, respectively), low *r*-values (0.867 and 0.904, respectively) were found, implying the importance of these solvent parameters. Conversely, omitting either SA or SB from the analysis (that is, with {SB, SP, SdP} and {SA, SP, SdP} as independent variables, respectively) gives excellent fits (*r* = 0.967 and 0.977, respectively). Further corroboration for SP and SdP as major factors comes from the six analyses with two solvent scales as independent variables: the analysis with {SP, SdP} yields the best fit (*r* = 0.964, Table S1), which is only fractionally lower than that for full analysis according to eq 1 (*r* = 0.979). That specific interactions (parameterized by {SA, SB}) have practically no influence on the position of $\bar{\nu}_{abs}$ is further corroborated by the unacceptable multi-linear fit of the

absorption maxima according to eq 1 with {SA, SB} as independent variables (r = 0.518).

Analogous analyses of the emission maxima of **6** also point to solvent dipolarity and polarizability as crucial factors determining the position of $\bar{\nu}_{em}$ (see Table S1).

Compound 10

The multi-linear analysis according to eq 1 (that is, with the {SA, SB, SP, SdP} solvent parameter set) of the $\bar{\nu}_{abs}$ data of **10** in the 12 solvents of Table 2 gives excellent fits (r = 0.994). The same was found for the corresponding analysis of the $\bar{\nu}_{em}$ data (r = 0.982). In order to find out which solvent properties principally account for the shifts of $\bar{\nu}_{abs}$ and $\bar{\nu}_{em}$, additional Catalán analyses according to eq 1 were carried out in which systematically one, two, and three solvent scales were omitted. From this multitude of analyses, it is evident that solvent polarizability (SP) and solvent acidity (SA) are mainly responsible for the observed shifts (see Table S1).

Table S1. Estimated coefficients (y_0, a_{SA}, b_{SB}, c_{SP}, d_{SdP}; in cm^{-1}) and correlation coefficient (r) for the (multiple) linear regression analyses according to eq 1 of the absorption ($\overline{\nu}_{abs}$) and fluorescence emission maxima ($\overline{\nu}_{em}$) of **8**, **6**, and **10** as a function of the Catalán solvent scales {SA, SB, SP, SdP} for the solvents listed in Table 2.

		y_0	c_{SP}	d_{SdP}	a_{SA}	b_{SB}	r
8	$\overline{\nu}_{abs}$	24761 ± 460	-1486 ± 590	942 ± 112	-337 ± 221	471 ± 144	0.951
	$\overline{\nu}_{abs}$	24705 ± 478	-1367 ± 609	909 ± 115		377 ± 136	0.943
	$\overline{\nu}_{abs}$	25446 ± 468	-2214 ± 623	954 ± 134			0.914
	$\overline{\nu}_{abs}$	23647 ± 85		957 ± 125		529 ± 131	0.924
	$\overline{\nu}_{abs}$	23808 ± 103		1097 ± 164			0.845
	$\overline{\nu}_{em}$	21898 ± 550	-953 ± 705	555 ± 134	-11 ± 264	873 ± 172	0.933
	$\overline{\nu}_{em}$	21896 ± 531	-949 ± 677	554 ± 127		870 ± 151	0.933
	$\overline{\nu}_{em}$	21161 ± 88		587 ± 129		975 ± 134	0.924
6	$\overline{\nu}_{abs}$	19245 ± 186	-1253 ± 211	197 ± 40	-112 ± 55	-68 ± 72	0.979
	$\overline{\nu}_{abs}$	19046 ± 104	-1014 ± 134	192 ± 37			0.964
	$\overline{\nu}_{em}$	18447 ± 297	-837 ± 337	170 ± 64	-69 ± 88	70 ± 114	0.933
	$\overline{\nu}_{em}$	18577 ± 136	-959 ± 175	135 ± 49			0.923
10	$\overline{\nu}_{abs}$	22690 ± 210	-1312 ± 239	258 ± 45	696 ± 62	50 ± 81	0.994
	$\overline{\nu}_{abs}$	23041 ± 222	-1578 ± 308		830 ± 132		0.961
	$\overline{\nu}_{em}$	20832 ± 248	-1094 ± 281	85 ± 53	365 ± 73	134 ± 95	0.982
	$\overline{\nu}_{em}$	21180 ± 122	-1444 ± 170		390 ± 73		0.974

^{1}H-NMR of 7 in $CDCl_3$

Table S2. Rate constants and free enthalpy of activation at the coalescence temperature T_c for **7**.

Peak	$\Delta\nu$ (Hz)	k_c (s^{-1}) (s^{-1})	T_c (K)	$\Delta G_c^{\neq}$ (kJ mol^{-1})
1,7-H	811	1800	238	43.0
2,6-H	127	282	228	44.6
3,5-H	/	/	/	/

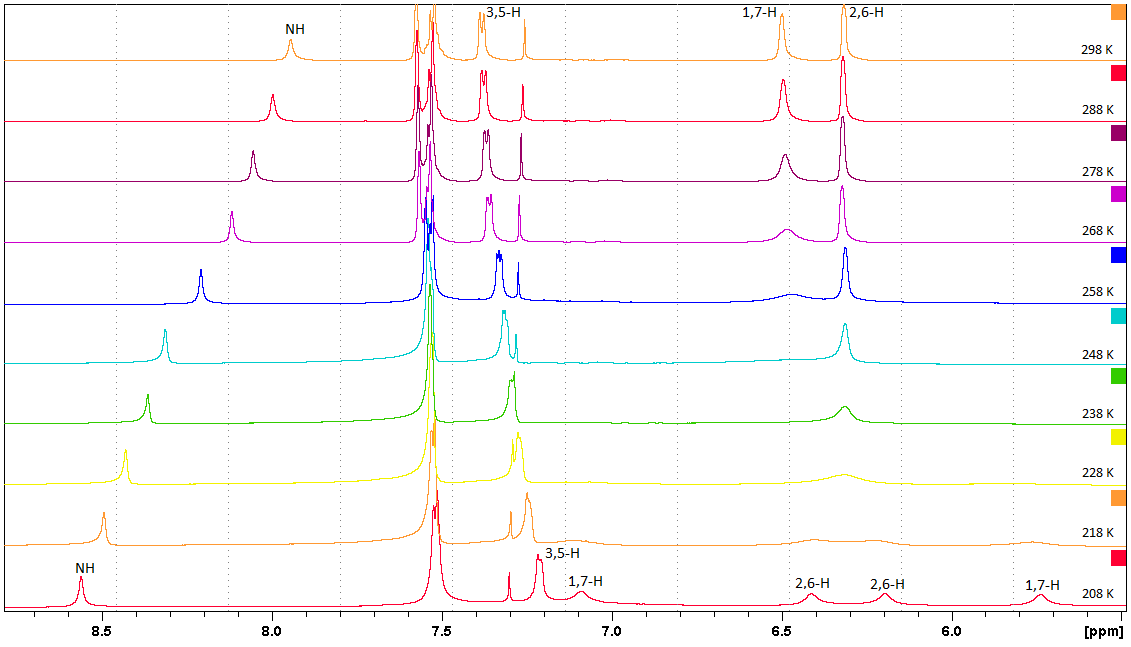

Figure S6. Aromatic region of the temperature dependent ^{1}H-NMR spectra of **7** measured in $CDCl_3$ at 600 MHz from 25 °C (top) to –65 °C (bottom).

^{1}H COSY NMR of 8 in $CDCl_3$

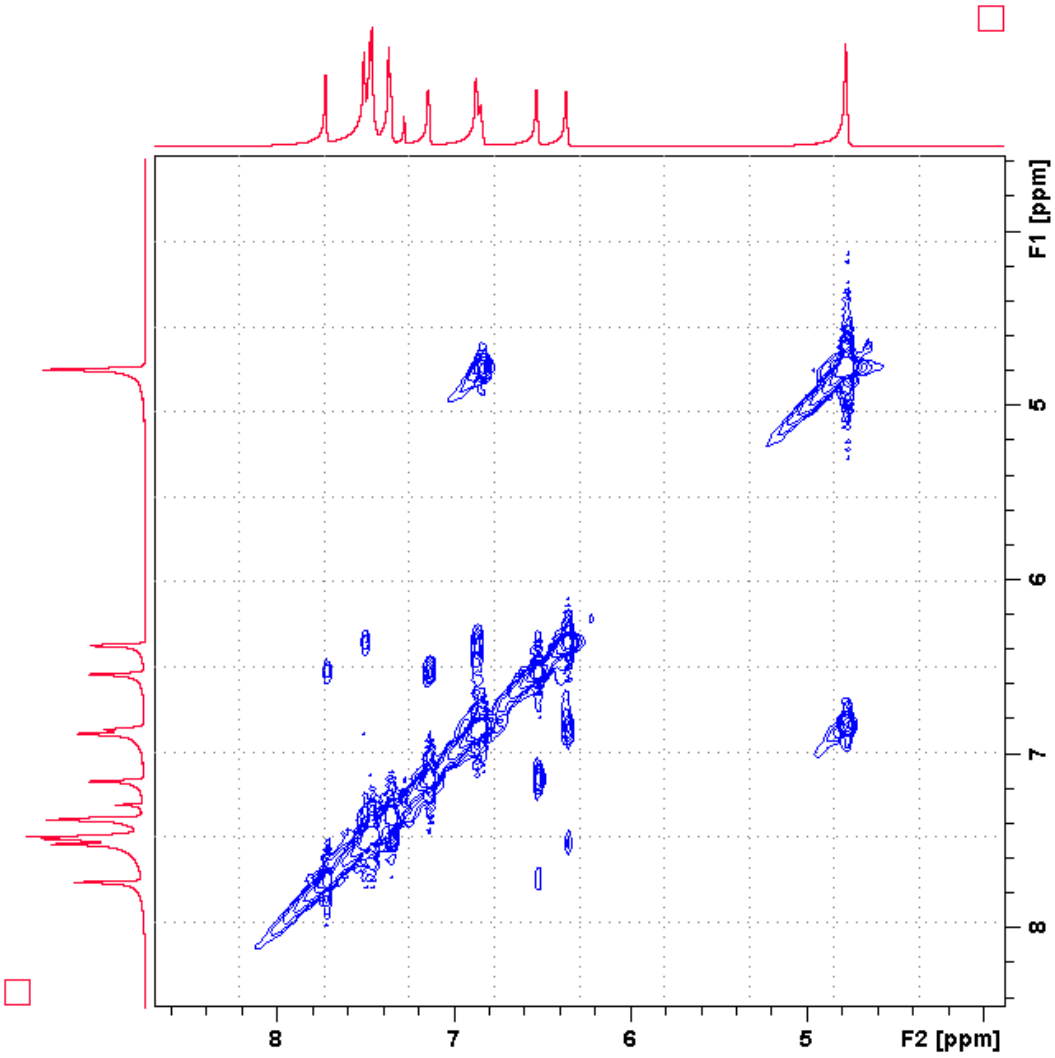

Figure S7. ^{1}H COSY NMR of **8** measured in $CDCl_3$ at 600 MHz at –25 °C to illustrate the coupling between pyrrole hydrogens and between CH_2 and NH.

^{1}H-NMR of 8 in DMSO-d_6

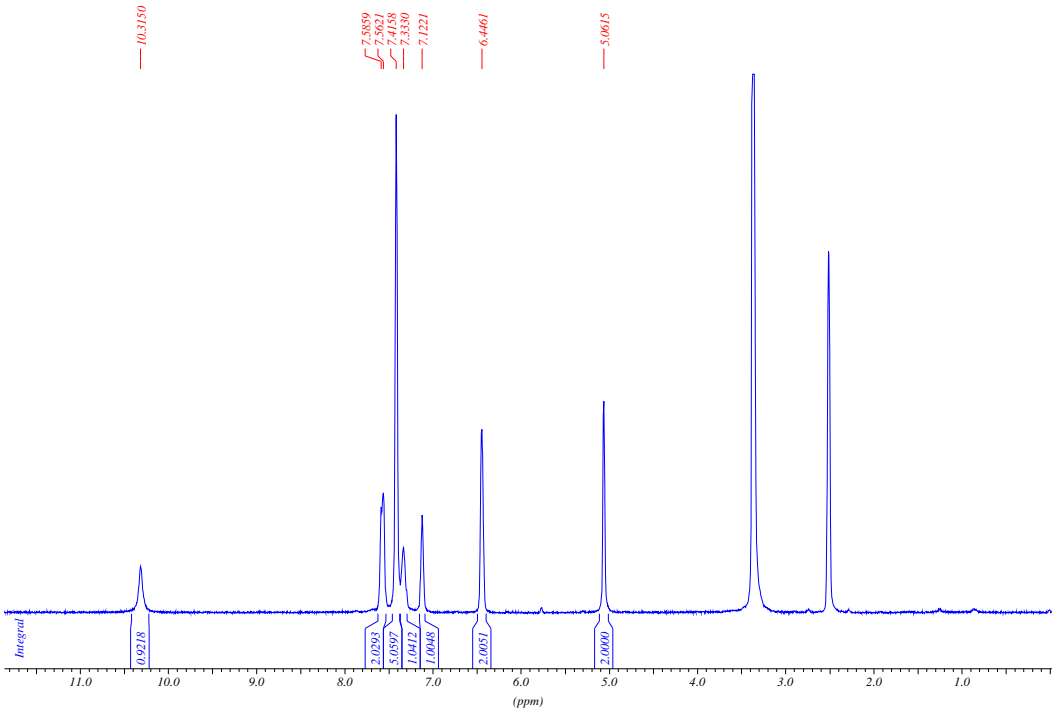

Figure S8. ^{1}H-NMR spectrum of **8** measured in DMSO-d_6 at 300 MHz at room temperature.

Quantum chemical calculations

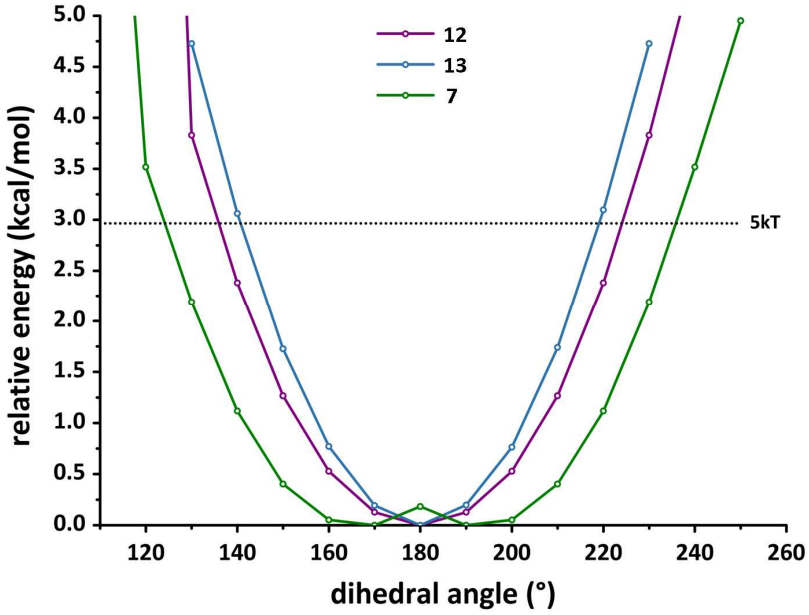

Figure S9. Potential energy surfaces of the ground state of **7**, **12**, and **13** as a function of the scanned dihedral angle between the BODIPY core and the *meso*-substituent plane.

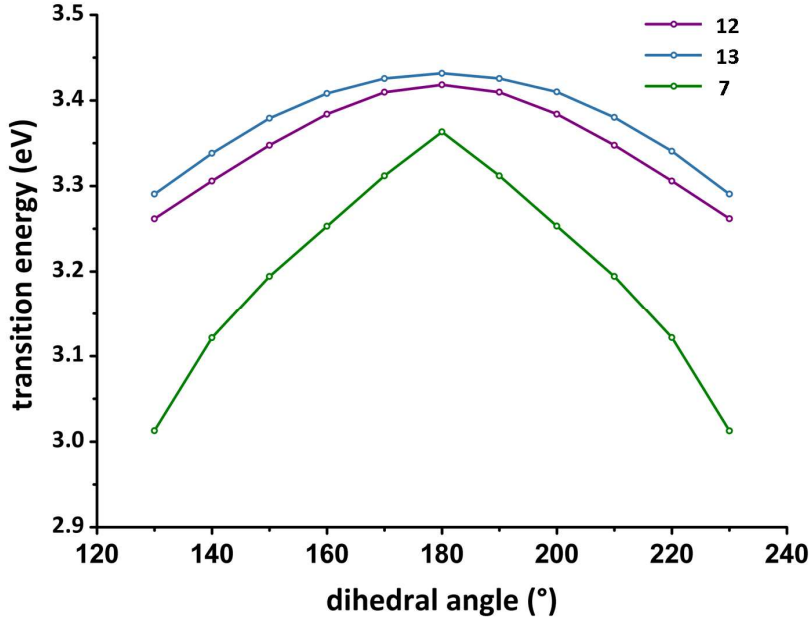

Figure S10. Evolution of the transition energy of **7**, **12**, and **13** as a function of the scanned dihedral angle between the BODIPY core and *meso*-substituent plane.

Crystallographic data for 7, 8, and 10

Table S3. Crystallographic data for **7**, **8**, and **10**, measured in this work.

	7[a]	**8**	**10**
Formula	$C_{15}H_{12}BF_2N_3$	$C_{16}H_{14}BF_2N_3$	$C_{15}H_{11}BF_2N_2O$
M (g/mol)	283.09	297.11	284.07
Space group	P-1 (no. 2)	P-1 (no. 2)	P-1 (no. 2)
a (Å)	9.7482(7)	11.5992(16)	5.5578(5)
b (Å)	11.7291(12)	11.690(2)	10.8386(10)
c (Å)	12.1757(10)	11.7664(16)	11.0174(10)
α (°)	97.176(8)	86.369(13)	87.304(8)
β (°)	105.473(7)	77.675(12)	79.109(7)
γ (°)	96.047(7)	63.181(16)	78.784(8)
V (Å^3)	1317.10(19)	1390.1(4)	639.24(10)
Z	4	4	2
T (K)	100	100	100
ρ_{calcd} (g cm^{-3})	1.428	1.420	1.476
μ(Mo Kα) (mm^{-1})	0.106	0.104	0.113
F(000)	584	616	292
Crystal size (mm^3)	0.2 × 0.2 × 0.2	0.2 × 0.2 × 0.2	0.3 × 0.2 × 0.2
Reflections measured	5366	5666	2593
Unique reflections	4391	4859	2167
R(int)	0.0208	0.0191	0.0214
wR_2 (all data)	0.0966	0.1033	0.0941
R_1 (>2sigma(I))	0.0402	0.0423	0.0407
CCDC deposition no	CCDC 961709	CCDC 961710	CCDC 961708

[a] The crystal structure of **7** has been reported before by Goud et al.[12] (CSD reference codes GEGGEF and GEGGEF01).

References

(1) Agilent **2012**, CrysAlis PRO. Agilent Technologies, Yarnton, Oxfordshire, England.

(2) Dolomanov, O. V.; Bourhis, L. J.; Gildea, R. J.; Howard, J. A. K.; Puschmann, H. *OLEX2*: A Complete Structure Solution, Refinement and Analysis Program. *J. Appl. Cryst.* **2009**, *42*, 339–341.

(3) Sheldrick, G. M. A Short History of *SHELX*. *Acta Cryst.* **2008**, *A64*, 112–122.

(4) Dimroth, K.; Reichardt, C.; Siepmann, T.; Bohlmann, F. Über Pyridinium-*N*-phenol-betaine und ihre Verwendung zur Charakterisierung der Polarität von Lösungsmitteln (Pyridinium-*N*-phenol-betaine and its Application for the Characterization of Solvent Polarities). *Liebigs Ann. Chem.* **1963**, *661*, 1–37.

(5) Dimroth, K.; Reichardt, C. Über Pyridinium-*N*-phenol-betaine und ihre Verwendung zur Charakterisierung der Polarität von Lösungsmitteln, V Erweiterung der Lösungsmittelpolaritätsskala durch Verwendung Alkyl-substituierter Pyridinium-*N*-phenol-betaine (Pyridinium-*N*-phenol betaines and their Application for the Characterization of Solvent Polarities. Extension of the Solvent Polarity Scale by Application of Alkyl-substituted Pyridinium-*N*-phenol Betaines). *Liebigs Ann. Chem.* **1969**, *727*, 93–105.

(6) Reichardt, C. Solvatochromism, Thermochromism, Piezochromism, Halochromism, and Chiro-solvatochromism of Pyridinium *N*-phenoxide Betaine Dyes. *Chem. Soc. Rev.* **1992**, *21*, 147–153.

(7) Kamlet, M. J.; Abboud, J. L.; Taft, R. W. The Solvatochromic Comparison Method. 6. The π* Scale of Solvent Polarities. *J. Am. Chem. Soc.* **1977**, *99*, 6027–6038.

(8) Dragos, R. S. Extension of the Unified Scale of Solvent Polarities to Acceptor Probes: Concerns about β–π* Parameters. *J. Org. Chem.* **1992**, *57*, 6547–6552.

(9) Catalán, J.; López, V.; Pérez, P.; Martin-Villamil, R.; Rodriguez, J. G. Progress Towards a Generalized Solvent Polarity Scale: The Solvatochromism of 2-(Dimethylamino)-7-nitrofluorene and its Homomorph 2-Fluoro-7-nitrofluorene. *Liebigs Ann.* **1995**, 241–252.

(10) Catalán, J. Toward a Generalized Treatment of the Solvent Effect Based on Four Empirical Scales: Dipolarity (SdP, a New Scale), Polarizability (SP), Acidity (SA), and Basicity (SB) of the Medium. *J. Phys. Chem. B* **2009**, *113*, 5951–5960.

(11) Valeur, B.; Berberan-Santos, M. N. *Molecular fluorescence. Principles and applications*, Wiley-VCH: Weinheim (Germany), 2nd ed., 2012.

(12) Goud, T. V.; Tutar, A.; Biellmann, J.-F. Synthesis of 8-Heteroatom-substituted 4,4-Difluoro-4-bora-3a,4a-diaza-*s*-indacene Dyes (BODIPY). *Tetrahedron* **2006**, *62*, 5084–5091.